Muon tagging using a Match-χ^2 based Soft Muon Tagger in top quark analyses using data from the ATLAS detector

Jacobo Ezequiel Blanco

Department of Physics

Royal Holloway, University of London

A thesis submitted to the University of London for the Degree of Doctor of Philosophy

April 16, 2014

DECLARATION

I confirm that the work presented in this thesis is my own. Where information has been derived from other sources, I confirm that this has been indicated in the document. Jacobo Ezequiel Blanco

Abstract

This is an abstract

Contents

List of Figures

List of Tables

Chapter 1

Introduction and motivation

This part will include an overview summary of the body of work presented in the thesis including a scientific motivation for the use of the soft muon tagger as a method for b-jet tagging and muon tagging.

Chapter 2

The Standard Model of Particle Physics

Particle physics is the study of the most fundamental consituents of matter and their interactions. The best current description of these interactions is known as The Standard Model of Particle Physics (SM); a group of theories that cover all currently known particles and their interactions. The SM was developed through-out the latter half of the 20th century and has seen tremendous success in predicting the behaviour of our universe at the most fundamental level. The SM has stood the test of time and rigorous examination by numerous experiments. The last piece to be confirmed was the existence of the Higgs boson, which in turn points to the existence of the so-called Higgs field. Evidence of the elusive Higgs were observed by the ATLAS and CMS experiments at CERN in the latter half of 2013.

The SM describes the nature of the interactions of the fundamental constituents of our universe in terms of the three different fundamental forces: Strong, Weak and Electromagnetic each described by a specific theory. Note that the most familiar of the forces, gravity, is not included in this list. The Standard Model does not incorporate a description of gravity, however the development of such description is the subject of much interest for those creating theories that go Beyond the Standard Model (BSM).

The Standard Model classifies particles into several categories depending on their properties and allowed interactions. Particles which have a half-integer spins (e.g. $\frac{1}{2}$,

$\frac{3}{2}$,...) are known as Fermions, and particles with integer spins (e.g. 0, 1,...) are known as Bosons. A summary of all elementary particles described by The Standard Model can be found in Table 2.1.

Fermions can be divided into two subgroups: Quarks, which can interact by the strong, weak and electromagnetic forces and leptons which can only interact by the weak and electromagnetic forces. Each group contains six particles which are categorized into 3 distinct generations. For every matter fermion (f) there is an equivalent antimatter partner ($\bar{f}$) which possesses the same characteristics as its matter companion but is opposite in electrical charge. Thus 12 matter particles are combined with 12 antimatter partners for a total of 24 elementary particles which form all material in the universe.

The interaction between fermions are occur via the exchange of spin one particles known as bosons. Each force is mediated by one or more bosons (Table 2.2). The strong force is mediated by a set of massless bosons known as the gluons. The weak force is mediated by a neutral massive boson known as the Z boson and a pair of charged massive bosons known as the W bosons. Finally, the elecromagentic force is mediated by a massless boson known as the photon. From Note that each boson has an antimatter partner however some are indistinguishable form their matter partner. A summary of their properties is show in Table 2.1.

2.1 Quantum Electrodynamics

The interaction of particles via the electromagnetic force is described by Quantum Electrodynamics or QED. These interactions are mediated by the massless neutral boson known as the photon and the strenght of the interaction is characterized by the fine-structure constant α. All electrically charged fermions are allowed to interact, however since the photon itself is not charged, no self-interaction is allowed within QED. One of the simplest examples of QED interactions is the decay of a photon into a fermion/antifermion pair (Figure 2.1). Note that the electric charge is conserved across the vertex, so for example $\gamma \to e^+e^+$ is not allowed within QED.

By combining different forms of this vertex one can build every possible QED interaction. Electron-Positron pairs can annihilate to create energy in the form of a photon

Table 2.1: A summary of all elementary particles described by The Standard Model. Note the various groupings and divisions including by spin, generation and particle type. Within the fermion sector the quarks are shown in yellow and the leptons are shown in green. These are grouped into three different generations traditionally denoted by roman numerals. The force mediators known as gauge bosons are shown in blue and finally the recently discovered Higgs boson with a spin of zero.

	Fermions ($s = \frac{1}{2}$) I	II	III	Bosons ($s = 0$)	Higgs ($s = 1$)
Quarks	$+\frac{2}{3}$ 2.3 MeV u Up	$+\frac{2}{3}$ 1.275 GeV c Charm	$+\frac{2}{3}$ 173.07 GeV t Top	0 0 MeV γ Photon (EM)	0 126.07 GeV H^0 Higgs boson
	$-\frac{1}{3}$ 4.8 MeV d Down	$-\frac{1}{3}$ 95 MeV s Strange	-$\frac{1}{3}$ 4.18 GeV b Bottom	± 1 80.4 GeV $W^{\pm}$ W boson (Weak)	
Leptons	-1 0.511 MeV e Electron	-1 105.7 MeV μ Muon	-1 1.777 GeV τ Tau	0 91.2 GeV Z Z boson (Weak)	
	0 < 2.2 eV ν_e Electron Neutrino	0 < 0.17 MeV ν_μ Muon Neutrino	0 15.5 MeV ν_τ Tau Neutrino	0 0 MeV g Gluon (Strong)	q mass **symbol** name (force)

Table 2.2: A summary of the four fundamental forces ordered by relative strength. These are approximated relative strengths for the purpose of demonstrating the hierarchy of forces as a function of their strength. A more accurate determination of the interaction strength depends on the details of the interaction itself. Note however the order-of-magnitude differences in the relative strengths of these forces. Note that the graviton is the theoretical boson responsible for mediating gravitational interactions, it is not part of the SM.

Name	Relative Strength	Boson
Strong	10^{38}	Gluons
Electronmagnetic	10^{36}	Photon
Weak	10^{25}	$W^{\pm}$and Z^0
Gravity	1	Graviton*

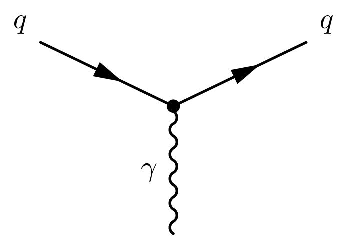

Figure 2.1: The interaction vertex described by QED. One can obtain all possible vertex shapes by rotating this basic vertex and assigning the appropriate electric charge and making sure to conserve lepton flavour across the vertex.

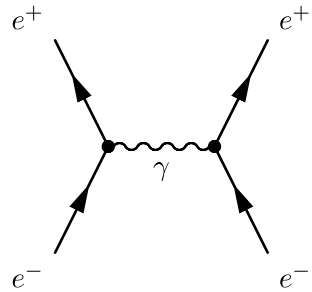

(a) Electron-Positron pair annihilation mediated by a photon.

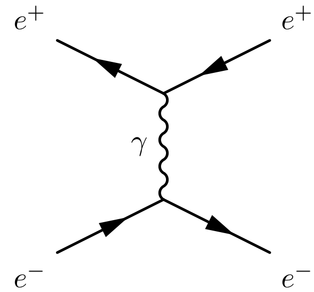

(b) Electron-Positron pair scattering via the emission of a photon.

Figure 2.2: Feynman diagrams of the process $e^+e^- \rightarrow e^+e^-$ allowed in QED. Note that these are the simplest diagrams, also known as tree level diagrams, and additional vertexes can be added to produce higher-order diagrams of the same process.

(Figure 2.2a) and then subsequently decay into an additional Electron-Positron pair. Electrons can scatter by emitting a photon which is then absorbed by a positron (Figure 2.2b) this processis known as Bhabha scattering.

2.2 Quantum Chromodynamics

Interactions via the strong force are described in the theory of Quantum Chromodynamics or QCD. These interactions are mediated by a set of massless neutral bosons known as gluons. QCD introduces the concept of "colour", which similarly to electrical charge, determines the possible interactions that can occur via the strong force. "Colour" can take three states red (antired), blue (antiblue), green (antigreen). Both quarks and gluons possess colour and as a result gluons, unlike photons, can self-interact (Figure 2.3)). As with electrical charge, colour-charge must also be conserved. Thus in the scattering process $q \rightarrow q + g$ shown in Figure 2.3a the flavour of the quark may not change but

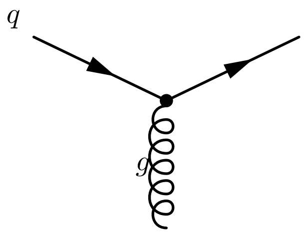

(a) Quark-gluon vertex.

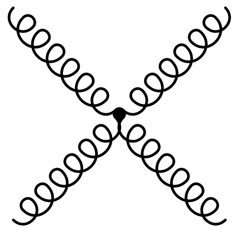

(b) Four-gluon vertex

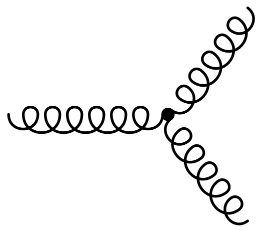

(c) Three-gluon vertex

Figure 2.3: Diagrams of the fundamental interaction vertices described by quantum chromodynamics.

the colour-charge does and the gluon carries away the difference in colour. There are eight different gluons that can participate in QCD interactions each with a different colour-charge combination. Note that there is a ninth combination ($R\overline{R} + G\overline{G} + B\overline{B}$) which is overall colorless so it cannot take part in interactions.

In an analogous fashion to screening which occurs with electric charges, quark-antiquark pairs act like dipoles which screen the true colour charge of the central quark. However since gluons also carry colour, they have the opposite effect of anti-screening which amplify and change the observed colour of the quark. Which effects wins out depends on the number of colours in the theory and the number of quark flavours. As it is with three colour states and six different quark flavours, anti-screening is the overall dominant effect. As a result the colour potential decreases with distance and quarks experience very little potential when very near to eachother. This effect is known as asymptotic freedom and results in quarks only existing within colorless bound states known as hadrons.

Hadrons can be divided into two categories: Mesons, which contain a quark and an antiquark ($q\overline{q}$); and Baryons which are made of three quarks (or antiquarks) each with a different (anti)colour-charge to result in a colourless composite particle. Common examples of baryons are protons (uud) and neutrons (udd) which are the building blocks of atomic nuclei.

2.3 Weak Interactions

The final type of interaction involves the so-called weak force. The weak force is responsible for β^- decay ($n \to p + e^- + \overline{\nu}_e$) and β^+ decay ($p \to n + e^+ + \nu_e$). Interactions via

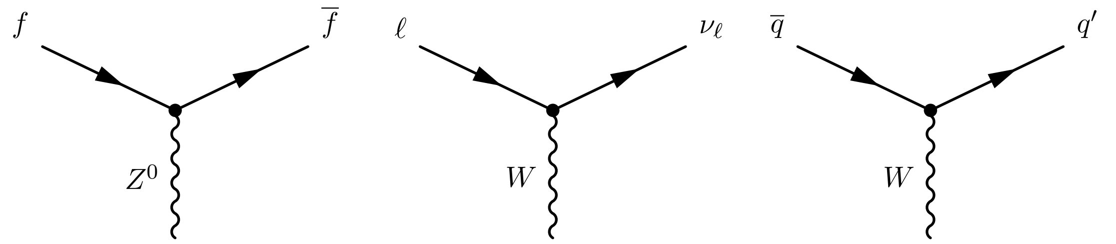

(a) Neutral current weak vertex (b) Charged current vertex involving leptons (c) Charged current vertex involving quarks

Figure 2.4: The neutral current and charged current vertexes allowed via the Weak force. Where f can be an e, μ or τ and ν_ℓ is the corresponding lepton neutrino of the same flavour. One can obtain all possible vertex shapes by rotating these basic vertexes and assigning the appropriate electric charge and making sure to conserve lepton flavour across the vertex.

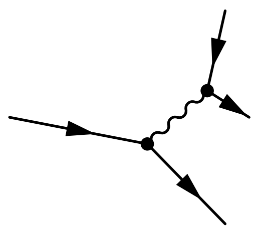

Figure 2.5: Neutral current weak scattering vertex

the Weak force are mediated by a single neutral massive boson and two charged massive bosons. Since the bosons responsible for weak interactions are massive, the range of interaction is very short, unlike electromagnetic interactions via a massless photon.

All fermions can take part in interactions via the Weak force. Interactions involving only leptons are simpler so we shall begin our review there. The Weak neutral vertex is very similar to the basic vertex seen in QED (2.1) A valid interactions via the weak force is then formed by combining these simple vertexes (Figure 2.4) while taking care to conserve electric charge and lepton flavour. An example of a leptonic weak interaction is muon decay ($\mu \to \nu_\mu W^- \to \nu_\mu e^- \overline{\nu}_e$) shown in Figure 2.5.

The Weak interactions is relatively simple and straight-forward as far as leptons are concerned. Things are not so when including quarks in weak interactions. The neutral vertex is similar to that of the leptonic version, a quark can emit a Z boson or a Z boson can decay forming a quark-antiquark pair. The charged current then changes the flavour of an up-type quark into a down-type quark (or vice-versa) with a W boson of the appropriate charge (Figure 2.4c). It is possible for a Weak interaction to change the flavour of a quark across families. A well known example of such an interaction is Kaon decay ($K^+ \rightarrow \mu^+\nu_\mu$). In order to account for this interaction and preserve the universality of weak interactions, Nicola Cabibbo postulated that the states that the states that couple to the charged current are really a mixture of 'rotated' quark states:

$$\begin{pmatrix} u \\ d' \end{pmatrix} \begin{pmatrix} c \\ s' \end{pmatrix} \begin{pmatrix} t \\ b' \end{pmatrix} \tag{2.1}$$

where

$$d' = d\cos\theta_c + s\sin\theta_c \tag{2.2a}$$

$$s' = -d\sin\theta_c + s\cos\theta_c \tag{2.2b}$$

This introduces an arbitrary parameter into the theory known as the quark mixing angle or the Cabibbo angle, named after Nicola Cabibbo who developed the phenomenon of quark mixing. The introduction of quark mixing has the effect of attenuating the interaction strength at vertexes involving multiple quark generations. Interactions which cross one generation ($u \rightarrow s$) are said to be Cabibbo Suppressed while those that cross two generations ($u \rightarrow b$) are Doubly Cabibbo suppressed.

Taking into account the three quark generations, quark mixing can be expressed in matrix notation as shown in Equation 2.3. This unitary matrix is known as the Cabibbo-Kobayashi-Maskawa Matrix (CKM Matrix) after Cabibbo which initially postulated quark mixing and Makoto Kobayashi and Toshihide Maskawa who later added an additional generation, containing the top and bottom quarks, to the matrix.

$$\begin{pmatrix} d' \\ s' \\ b' \end{pmatrix} = V_{CKM} \begin{pmatrix} d \\ s \\ b \end{pmatrix} = \begin{pmatrix} V_{ud} & V_{us} & V_{ub} \\ V_{cd} & V_{cs} & V_{cb} \\ V_{td} & V_{ts} & V_{tb} \end{pmatrix} \begin{pmatrix} d \\ s \\ b \end{pmatrix} \tag{2.3}$$

The elements of the CKM matrix have been measured and the latest accepted results are summarized in 2.5. The interaction strength is then proportional to $|V_{ij}|^2$. Including all three generations the sum of all possible transitions from a given quark, q, is unity:

$$\sum |V_{qi}|^2 = 1 \tag{2.4}$$

Note that the term V_{tb} is approximately unity and by far dominates over the other V_{tj} terms. This means that the top-quark transitions almost exclusively into a b-quark ($t \to Wb$) with transitions $t \to Ws$ and $t \to Wd$ being exceedingly rare. The Soft Muon Tagger which is the focus of this thesis relies on Weak semileptonic decays of b-quarks. From 2.5 one can see that the transition $b \to c$ dominates over $b \to u$.

$$V_{CKM} = \begin{pmatrix} 0.97427 \pm 0.00015 & 0.22534 \pm 0.00065 & 0.00351^{+0.00015}_{-0.00014} \\ 0.22520 \pm 0.00065 & 0.97344 \pm 0.00016 & 0.0412^{+0.0011}_{-0.0005} \\ 0.00867^{+0.00029}_{-0.00031} & 0.0404^{+0.0011}_{-0.0005} & 0.999146^{+0.000021}_{-0.000046} \end{pmatrix} \tag{2.5}$$

An additional unique feature of Weak interactions is that the charge conjugation-parity (CP) symmetry is violated. The operator C denotes the change of a particle by its antiparticle partner and P denotes a reversal of helicity (the projection of spin onto the momentum of a particle). A clear violation of C and P was observed in the radioactive decay of Cobalt-60, where the resulting electrons were preferentially emitted in the opposite direction of the nuclear spin of the Cobalt. Thus weak currents only couple to left-handed neutrinos (or right-handed antineutrinos) this is then a violation of parity. Additionally charge symmetry is also violated since a left-handed neutrino is preferentially picked over a left-handed antineutrino. Finally in 1964 CP violation was observed in the decay of neutral kaon.

Thus the probability of $\overline{a} \to \overline{b}$ is not equal to that of $a \to b$. The existence of CP violation has interesting consequences for the formation of the early universe. The preferential production of matter over antimattter in CP violating interactions would shift the balance in favour of matter resulting in a universe similar to our own.

2.3.1 Electroweak Unification and the Higgs mechanism

Chapter 3

Top-quark physics

Since this thesis will focus mostly on top quark physics a strong emphasis is put on the description of processes involving this quark

3.1 Top quark production

3.2 Top quark decay modes

Chapter 4

The LHC and the ATLAS Detector

This section will include a description of the Large Hadron Collider and the ATLAS detector technology with particular emphasis on those aspects that allow for precision measurement of muons and top quark physics studies.

4.1 The Large Hadron Collider

4.2 The ATLAS detector

Chapter 5

Identifying b-jet, and the Match χ^2 based Soft Muon Tagger

This section will include a description of several current methodologies for b-jet tagging and a detailed description of the Match-χ^2 Soft Muon Tagger.

5.1 b-jet tagging methodology

5.2 The Match-χ^2 Soft Muon Tagger

Chapter 6

Calibration of the Soft Muon Tagger for 2012 ATLAS Data

High-energy physics relies heavily on the use of simulated data to inform the development of analysis techniques. It is thus paramount that the simulation reflect nature as closely as possible. However the simulation does not accurately predict conditions within the detector and the effects on the muon reconstruction and the quality of the fit between the inner detector tracks and muon spectrometer tracks which is represented in the χ^2_{match}. Instead the difference between simulation and data is quantified and taken into account. This process is known as calibration. In the case of the muon reconstruction method and the χ^2_{match} tagger it is important that the difference in efficiency between MC and data be accounted for. This is done by constructing a scale factor, defined in this case by:

$$\kappa_{\chi^2_{\text{match}}} = \frac{\epsilon^{\text{Data}}_{\chi^2_{\text{match}}}}{\epsilon^{\text{MC}}_{\chi^2_{\text{match}}}} \tag{6.1}$$

One of the advantages of using the χ^2_{match} tagger over other forms of tagging is that the presence of a jet is not required to measure the χ^2_{match} of a muon. This means that the calibration can be performed on a isolated muons such as those from $J/\psi \to \mu\mu$ or $Z \to \mu\mu$ using the so called tag and probe method. This calibration relies on muons with low p_{T} from J/ψ decays. As the χ^2_{match} is a characteristic of combined and therefore reconstructed muons,

The tag and probe method used in this calibration is defined as follows. One reconstructed combined muon is designated as the Tag, this muon must pass a stringent set of cuts implying that this is indeed a muon from a J/ψ. The second muon which is designated as the Probe is constructed from an inner detector (ID) only. To ensure that the Probe is the second muon from the J/ψ decay, the invariant mass of the combined tag and probe system is required to be within a mass window centered around the true J/ψ mass. The complete selection used in the calibration is detailed in Section 6.1. These Probes are then used to measure the reconstruction efficiency and the χ^2_{match} tagger efficiency as described in Sections 6.2 and 6.3.

The tag and probe method used here is based on a previous calibration of the χ^2_{match} tagger performed on 2011 ATLAS collision data outlined in This analysis differs from the 2011 calibration in several ways these will be highlighted and explained.

6.0.1 Software, Collision Data and Simulated samples

The tag and probe method used here was implemented using the ROOT analysis framework.

The calibration was performed on a dataset made of those luminosity blocks selected by the recommended standard Good Runs List (GRL) which corresponds to all *pp* collision periods in 2012. The GRL selects only those luminosity blocks where detector conditions are appropriate for physics data-taking. This includes all relevant detector components being operational and that stable beam conditions have been achieved. The datasets are part of the 2013 summer reprocessing (processing tag p1328) corresponding to data taken in periods A through to L, excluding periods F and J.

The efficiency scale factor is measured against a sample containing almost 10 million $J/\psi \rightarrow \mu\mu$ events. At event generation filters are applied so the sample only contains events where both muons have a transverse momentum of at least 4 GeV and they must lie within the pseudo-rapidity range $|\eta| < 2.5$. This selection matches the object selection used by most analyses as recommended by the Muon Combined Performance (MCP) group.

6.1 Tag and Probe Selection

A tag and probe method was chosen to measure the efficiency of muon reconstruction and the χ^2_{match} tagger. The tag and probe method allows for the measurement of the performance of selection criteria or algorithms by exploiting well known decays. By creating a sample of objects, in this case muons, on which to apply the aforementioned selection criteria, it is possible to study these algorithms.

The muon reconstruction algorithm examines various Inner Detector (ID)tracks and Muon Spectrometer (MS) tracks and makes a determination as to whether said track is produced by muon or not. To measure the performance of the muon reconstruction algorithm a sample of ID tracks which originate from the J/ψ decay and are thus very likely to be a real muon is constructed. This is done in the following way:

First, require the presence of a combined `STACO` muon which passes a very stringent selection. This strongly implies that this is a real muon and thus is labelled as the Tag. Additionally a very loose selection is applied to all ID tracks. These are known as candidate Probes. Pairs of tag and probes are then formed by requiring that the combined invariant mass lie within a J/ψ mass window and the pair pass additional pairing cuts. This then implies that the Probe is likely the other muon from the J/ψ decay and as such is a suitable test-bed to measure the performance of the muon resconstruction algorithm. Note that all selection criteria are detailed and explained in Section 6.1.2

After selecting a sample of probes the performance of the algorithm is estimated by measuring the proportion of probe candidates which are selected by the algorithm. In other words the performance is estimated by counting the number of muons which are reconstructed given that the ID track is very likely to be a real muon. Probes which are reconstructed into combined `STACO` muons are labelled as muon probes. The performance of the χ^2_{match} tagger is estimated in a similar manner, by measuring the proportion of combined muon probes which pass the SMT selection.

6.1.1 Trigger requirements

In order for an event to be included in the analysis it must pass at least one of the trigger chains listed in Appendix A. For the sake of brevity only the primary trigger (`EF_mu6_Trk_Jpsi_loose`) which contributes the majority of events is described here.

As stated in the trigger name this is an Event Filter trigger which requires the presence of a muon with a momentum of at least 6 GeV and an ID track whos combined invariant mass lies within a J/ψ mass window of 2.6 GeV $< m_{\text{inv}} <$ 3.6 GeV. This loose mass window contains the entirety of the J/ψ peak in all examined p_T and η ranges as well as additional side bands to allow for background removal. Note the omission of double muon triggers to avoid introducing a bias by specifically selecting events with two good muons.

Also note that while all triggers are operational in all periods, most are heavily prescaled and the prescale is period dependent. This does not have a first-order effect on the measurement since only ratios are compared between collision data and MC.

6.1.2 Selection Cuts

The selection criteria for tags, probes, muon probes and SMT muons are listed and detailed below. Note that all cuts are applied on the kinematic properties measured in the ID due to its improved resolution unless it is not possible as in the case of the χ^2_{DoF} which is a combined MS and ID property. Also note that all objects must pass a selection criteria collectively refered to as MCP cuts. These are tracking quality cuts which require a certain number of detector elements be active to ensure good tracking. These cuts are listed in

The muon tag selection criteria are defined in the list below:

- MCP cuts
- `STACO` collection
- Combined muon
- p_T >4 GeV
- $|\eta|$ <2.5

- $|d_0|$ <0.3 mm and $|z_0|$ <1.5 mm
- $|d_0/\sigma_{d_0}|$ <3 and $|z_0/\sigma_{z_0}|$ <3
- Fired at least one of the relevant triggers (see Appendix A)

Included are cuts on the muon impact parameter (IP) d_0 and z_0. These are defined as the distance of closest approach of the ID track to the primary interaction vertex in the transverse and longitudinal planes, respectively. Additionally cuts on the absolute values of IP significances are also implemented. The signifiance of the impact parameter is defined as d_0/σ_{d_0} where σIP is the standard deviation of the impact parameter. These cuts are designed to ensure that the muon selected originates near the primary vertex and thus from a prompt J/ψ from the primary collision. Note that non-prompt J/ψ can be produced in the decay of b hadrons. Finally note that the tag muon must match the trigger object which selected this event.

The probe selection is a subset of the tag selection and only requires an ID track with $|\eta| < 2.5$ and $p_T < 4$ GeV. The pairing cuts are shown below:

- 2 GeV $\leq m_{\text{inv}} \leq$ 4 GeV
- Probe charge is opposite the tag charge
- 0.4 < ΔR(tag, probe)< 3.5
- Δz_0(tag, probe)< 0.2 mm

The probe and the tag are required to be fairly well separated to avoid the momentum of the tag from entering the isolation cone of the probe. In the 2011 calibration analysis the track of the tag and the probe are refit to a common vertex and the quality of the refit, expressed by the χ^2 is a part of the pairing criteria. This criteria is present to reduce the effects of pile-up on the measurement, by ensuring both objects have a common origin. Since the data format used for this analysis is a derived form of that used in 2011 it is not possible to perform such a refit. Instead the difference between the z_0 of the tag and the probe is used.

The `STACO` reconstruction efficiency is not measured by applying the algorithm on the probe collection but rather a probe is said to be a muon probe if it matches a combined muon from the `STACO` collection. This is done by requiring the angular separation between the probe and the `STACO` muon be less than 0.001. Probes which are matched become the numerator of the reconstruction efficiency and the denominator is defined as the number of probes:

$$\epsilon = \frac{N_{\text{muon probe}}}{N_{\text{probe}}}$$

A muon probe is said to be an SMT muon if it passes the following selection, which matches the muon cuts defined in Chapter 5

- $|d_0| < 3$ mm
- $|z_0 \sin(\theta)| < 3$
- $\chi^2_{\text{match}}/N_{\text{dof}} < 3.2$

Those muon probes which pass the SMT selection are the numerator of the SMT efficiency and the denominator is defined as the number of muon probes:

$$\epsilon = \frac{N_{\text{SMT}}}{N_{\text{muon probe}}}$$

6.2 Invariant mass fitting

The pairing criteria are very effective at selecting J/ψ events, however non-J/ψ background events are also pass the selection. These include combinatiorial background where the wrong tag and probe pair is constructed and Drell-Yan which appears as a continuum below the J/ψ peak.

The number of probes is extracted from a fit to the invariant mass of the dimuon system using a composite function to accomodate for the background and the gaussian-like J/ψ peak.

The invariant mass peak of the J/ψ is modelled by a gaussian distribution while the background distribution is modelled by a quadratic. The invariant mass distribution is fit by a sum of the two functions.

To avoid the first-order effects of signal mis-modelling from the fit of the J/ψ peak, the yield is obtained from the integral of the measured invariant mass distribution subtracting the background contribution from the integral of the fit to the background. The integration is performed in a window with a width based on the width of the fitted J/ψ peak. The integration window marked in Fig. 6.1 corresponds to three times the width of the peak or simply 3σ. Additionally note the composite fit line as well as the background-only distribution and the implied signal gaussian peak.

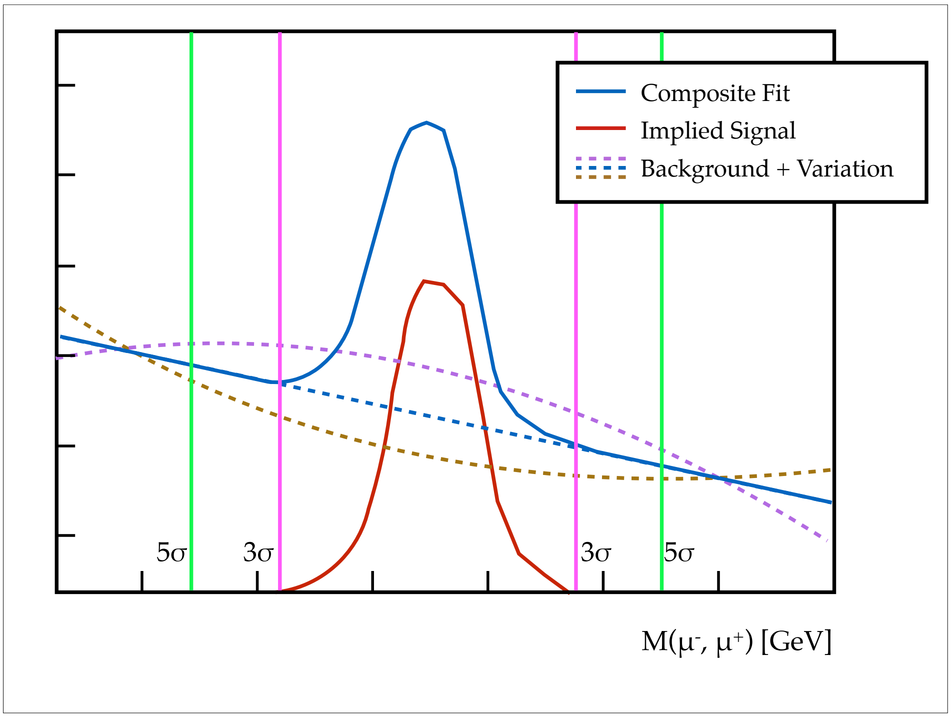

Figure 6.1: A diagram of the various components of the fit procedure. The composite fit is shown along with the corresponding implied signal and background. The two variations of the background shape are also shown.

6.2.1 Uncertainty Measurement

The uncertainty on the efficiency is made of three components. First, the statistical uncertainty on the efficiency is estimated as a Binomial error:

$$\delta\epsilon = \sqrt{\frac{\epsilon \times (1-\epsilon)}{N}} \tag{6.2}$$

Where ϵ is the measured efficiency and N is, in this case the denominator of the efficiency measured.

Secondly, an uncertainty is associated with the fit to the background. This is done by taking the largest upward and downward fluctuations of the background by the uncertainty on the fit parameters of the background, and obtaining the maximum upward and downward effects on the efficiency. After the fit of the composite function is carried out, a downward variation of the background is defined as:

$$f(x) = a_{\text{min}}x^2 + b_{\text{max}}x + c_{\text{min}}, \text{ where } p_{\text{max/min}} = p_{\text{central}} \pm \sigma_p \tag{6.3}$$

Here the maximum and minimum of a parameter is obtained by varying the central value by the uncertainty obtained from the fit. The upward variation of the background fit is thus the opposite, defined as:

$$f(x) = a_{\text{max}}x^2 + b_{\text{min}}x + c_{\text{max}} \tag{6.4}$$

These background variation then result in the maximum deviation from the nominal integral. Again Fig. 6.1 shows these two variations[1]. The uncertainty on the efficiency is then determined by obtaining the maximum efficiency in both directions. If the nominal efficiency is defined as:

$$\epsilon_{\text{nominal}} = \frac{N_{numerator}}{N_{denominator}} \tag{6.5}$$

Then the variations are defined as follows:

$$\epsilon_{\text{up}} = \frac{N^{down}_{numerator}}{N^{nominal}_{denominator}}, \ \epsilon_{\text{down}} = \frac{N^{nominal}_{numerator}}{N^{up}_{denominator}} \tag{6.6}$$

Finally the uncertainty on the background is given by adding the differences between ϵup and ϵdown and the nominal efficiency, in quadrature:

$$\sigma_{\text{bkg}} = \sqrt{|\epsilon_{\text{up}} - \epsilon|^2 + |\epsilon_{\text{down}} - \epsilon|^2} \tag{6.7}$$

The final component of the uncertainty is constructed by varying the integration

[1] The variation shown in the diagram is very exagerated and meant for illustration purposes

window. The nominal value is defined as 3σ away from the center of the fitted gaussian, where again σ is the FWHM of the same fitted gaussian. An uncertainty is constructed by measuring the efficiency with a wide integration window corresponding to 5σ. The integration window uncertainty is defined as:

$$\sigma_{\text{window}} = |\epsilon_{5\sigma} - \epsilon_{3\sigma}| \tag{6.8}$$

Finally, the total uncertainty on the efficiency is given by the sum in quadrature of the all uncertainty components. The uncertainty on the efficiency is then carried over to the scale factor determination.

An example of the fitting procedure applied is shown in Fig. 6.2 for both tag and probes at probe level and at muon probe level. Note that as expected the muon probe contains far less background.

6.3 Efficiencies

The efficiency is monitored as a function of a variety of kinematic variables, including isolation variables, transverse momentum and angular position of the probe.

6.3.1 Isolation dependence

The muons from J/ψ used in this calibration are produced in isolation, there is very little energetic activity surrounding them in the detector. In contrast muons from semileptonic decay of b-quarks in $t\bar{t}$ events are produced amongst the numerous components of the b-jets. Thus it is important to ensure that the performance of the χ^2_{match} tagger is not affected by the isolation of the muon for a calibration on J/ψ events to be applicable. In this calibration as, in the 2011 analysis nine isolation variables are considered. The so-called etcone20, 30 and 40 correspond to the transverse energy surrounding the muon in a cone of size $\Delta R = 0.2, 0.3, 0.4$ respectively. Additionally ptcone20, 30 and 40 and nucone20, 30, 40 correspond to the sum of transverse momentum and the number of tracks surrounding the muon, respectively. All nine isolation variables exclude the muon itself in a cone of size 0.1 and include various corrections for known energy losses, momentum leakages between adjacent clusters in the detector and the effects of pile-up.

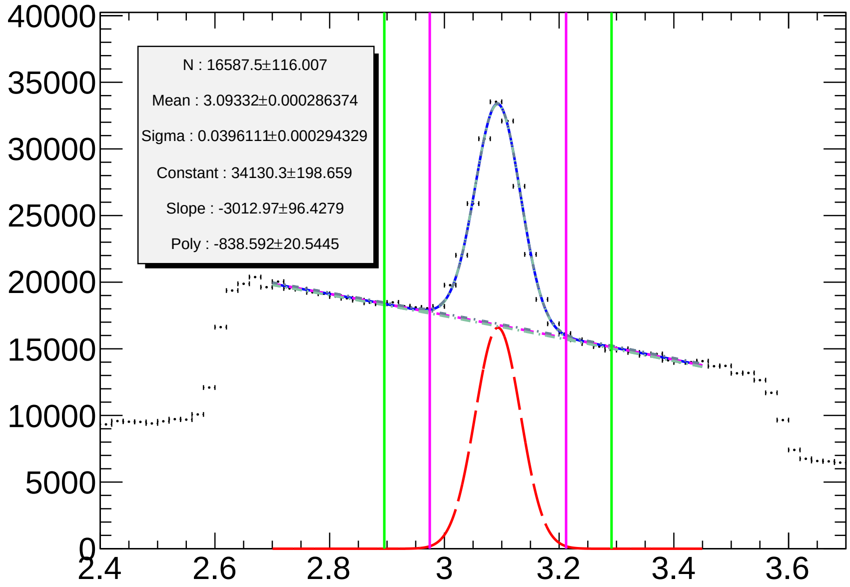

(a) Probe level

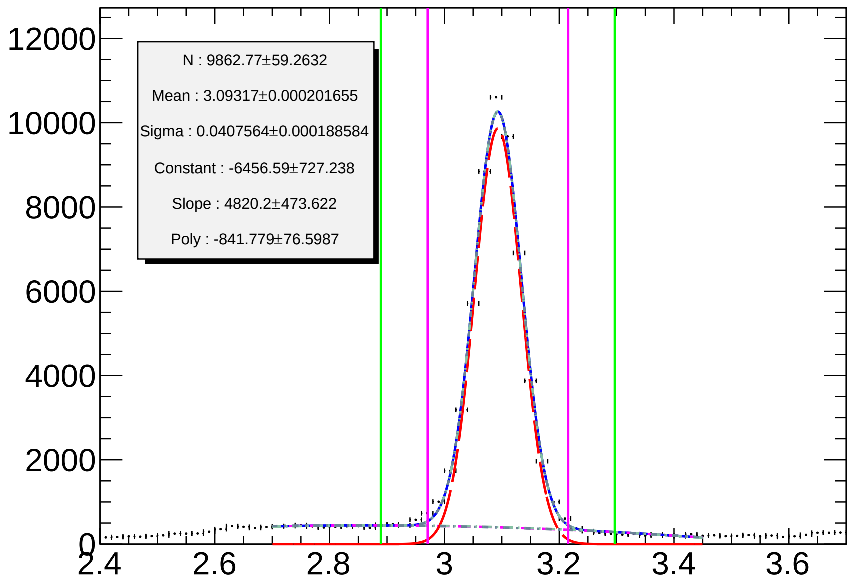

(b) Muon probe level

Figure 6.2: Invariant mass distributions of tag and probe pairs at a) probe level and at b) muon probe level in collision data. Note the various components of the fit as well as the variations on the background fits and the 3σ and 5σ integration windows used for systematics. Note the fit parameters and their respective uncertainties

As in the 2011 analysis there appears to be no dependence of the scale factor on any of the isolation variables examined as can be seen from Fig. 6.3.

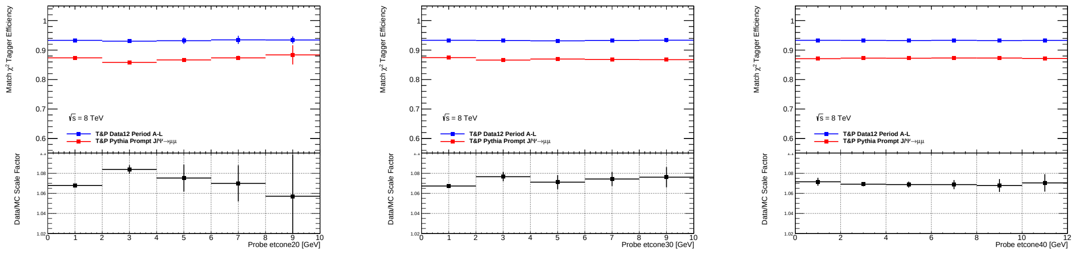

(a) $\sum E_T$ in cone $\Delta R = 0.2$ (b) $\sum E_T$ in cone $\Delta R = 0.3$ (c) $\sum E_T$ in cone $\Delta R = 0.4$

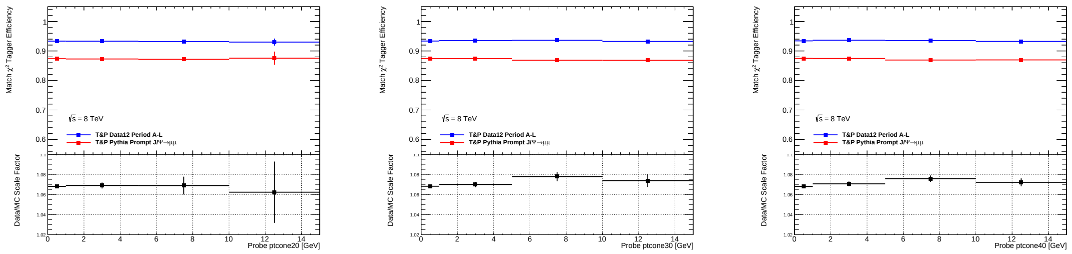

(d) $\sum p_T$ in cone $\Delta R = 0.2$ (e) $\sum p_T$ in cone $\Delta R = 0.3$ (f) $\sum p_T$ in cone $\Delta R = 0.4$

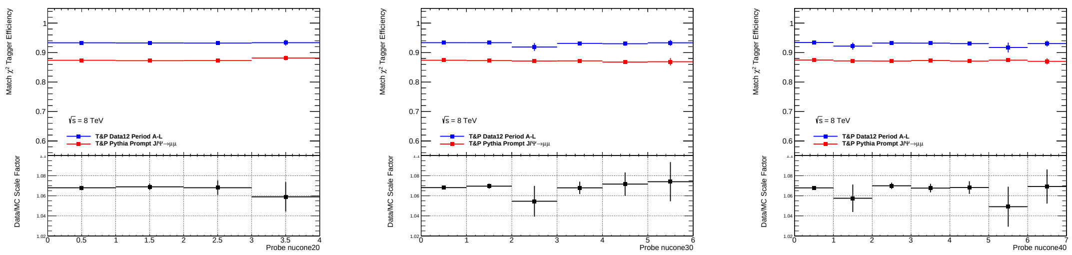

(g) N_{trk} in cone $\Delta R = 0.2$ (h) N_{trk} in cone $\Delta R = 0.3$ (i) N_{trk} in cone $\Delta R = 0.4$

Figure 6.3: χ^2_{DoF} efficiencies and scale factor with respect various isolation variables.

The dependence on each isolation variable is measured in a range dictated by the available statistics. Given the isolated nature of muons in J/ψ events limits the number of muons available at higher pt/et/nucone values.

6.3.2 2011 Calibration

6.3.3 Efficiency Binning

The efficiencies are measured across the $|\eta|$ range of the ATLAS detector in regions defined in Table 6.1. As in 2011, the efficiency is expected to be depedent on the region of the detector where the muon probe emerges.

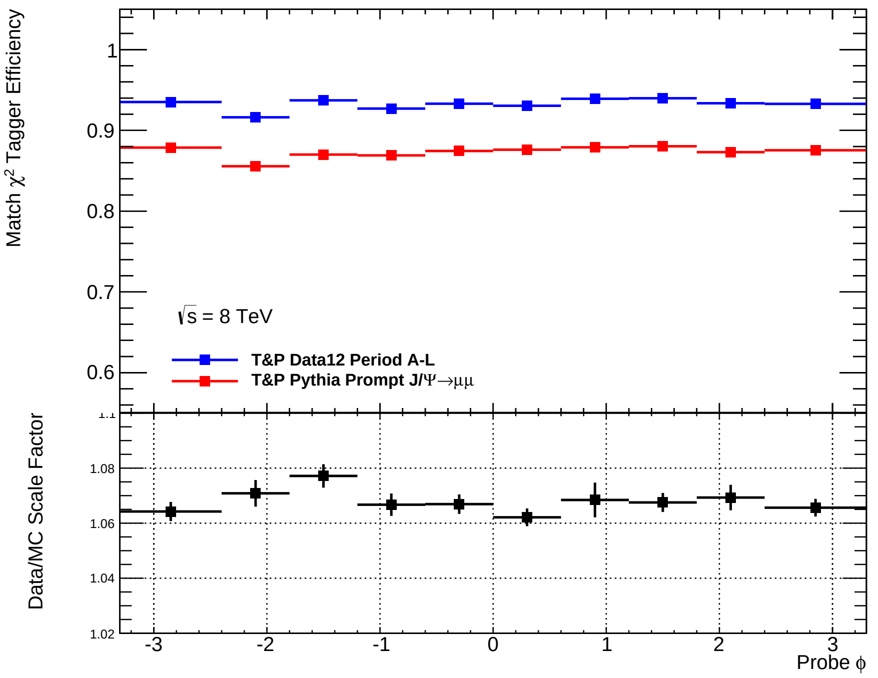

(a) χ^2_{match} efficiency and scale factor as a function ϕ of the probe muon

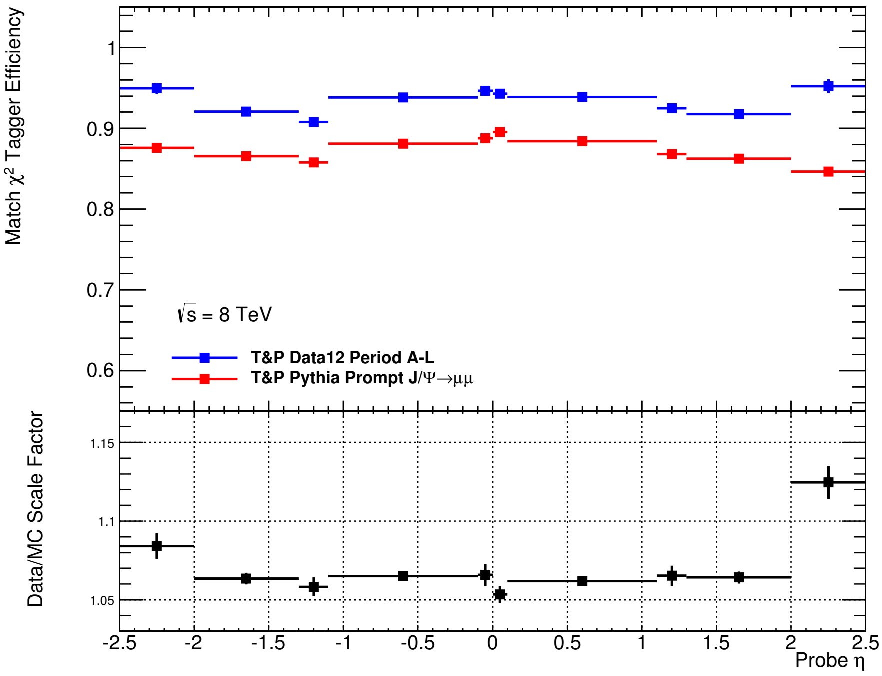

(b) χ^2_{match} efficiency and scale factor as a function η of the probe muon

Figure 6.4: χ^2_{match} efficiencies and scale factor with respect to the angular position of the muon probe

Table 6.1: Pseudorapidity regions of the ATLAS detector

$\|\eta\|$ range	Name
$0.0 < \|\eta\| < 0.1$	Crack
$0.1 < \|\eta\| < 1.1$	Barrel
$1.1 < \|\eta\| < 1.3$	Transition
$1.3 < \|\eta\| < 2.0$	Endcap
$2.0 < \|\eta\| < 2.5$	Forward

Chapter 7

Measurement of the $t\bar{t}$ cross-section in the single-lepton channel using SMT

This section will discuss the measurement of the $t\bar{t}$ cross-section in the single-lepton channel with an emphasis on the electron multijet background estimation conducted.

7.1 Data and Monte Carlo samples

This section will

7.2 Object selection and event selection

7.3 Re-weighting of the b-quark to muon transition BR

7.4 Data-driven background selection

7.5 Systematics uncertainties

7.6 Results and conclusion

Chapter 8

Muon Tagging in a boosted $t\bar{t}$ environment

The large center-of-mass energies at which collisions occur at the LHC allows for the production of very high mass particles. Several Beyond the SM (BSM) theories predict the existence of high mass particles which decay primarily top quark pairs. An example of hypothetical model which predict high mass $t\bar{t}$ resonances is the topcolor assisted technicolor model (TC2), which predicts the existence of a leptophobic Z' boson. The resultant top quark pair provides a well understood probe to search for such hypothetical particles.

The Z' could potentially have a mass on the order of several TeV. As a result their decay product would be produced in the detector with very large momentum. These top quarks are said to be boosted. In terms of the subsequent top decay, the resultant bottom quark and W boson are expected to emerge in a collimated cone. The events thus appear as two large back-to-back jets. If the W decays leptonically, the W lepton is expected to lie very close to or within the b-jet. If the W decays hadronically all three jets will appear to merge into a single 'fat' jet.

In this chapter the results of a feasibility study conducted to determine the viability of using the χ^2_{match} tagger to tag W muons from boosted top-quark decays is presented and discussed. Note that this is in contrast to the cross-section analysis detailed in a previous chapter where the muon tagged came from the semileptonic decay of b-quarks.

The boost is expected to be related to the mass of the Z' produced, so a higher mass Z' would decay into more collimated jets. The environment that results is thus very similar to that of a semileptonic b-decay, a muon buried inside of a b-jet.

No evidence for such a resonance has been observed and limits have been placed on the production rate of these resonance for various benchmark models. A leptophobic topcolor Z' of mass less than 1.74 TeV has been excluded using 4.7 fb^{-1} of pp collision data collected by ATLAS with a center-of-mass energy $\sqrt{s} = 7$ TeV [3]. Additionally a more recent analysis using 14.3 fb^{-1} of $\sqrt{s} = 8$ TeV data collected at ATLAS excluded a Z' with a mass less than 1.8 TeV at 95% confidence level [1]. The analysis detailed here is based on the 7 TeV analysis. Similar analyses performed with data collected by CMS have excluded Z' candidates for similar benchmark models [2, 4, 5].

The performance of SMT is compared to the contemporary method for selecting muons known as mini-isolation. In addition a short performance study to determine the viability of using SMT to tag b-jets in boosted top events is also presented. Firstly, a short examination of the topology of a boosted event is presented.

8.1 Boosted event topology

In order to perform an effective feasibility study, it is important to understand the signature left by boosted events in the detector. There are certain expectations regarding the momentum distribution of the various product particles from the decay of the top as well as their angular separation. As with the cross-section analysis presented in Chapter 7, this study focuses on the semileptonic decays of top quark pairs

It is expected for events where the momentum of the top quarks higher to exhibit stronger collimation between the W muon and the b-quark. This results in a situation very similar to that exploited for muon tagging in Section 7 where a muon from the semileptonic decay of a b-quark emerges from within the b-jet. Fig. 8.1 illustrates the similarity of both scenarios. It is thus possible to use the χ^2_{match}-tagger[1] to tag W muons in boosted events. As the tagger is designed to work in energetically "busy" sectors of the detector, it is ideally suited to probe highly boosted events where the decay products

[1]As signal muons are very hard, the tagger is now refered to as the χ^2_{match}tagger not soft muon tagger to reflect this difference

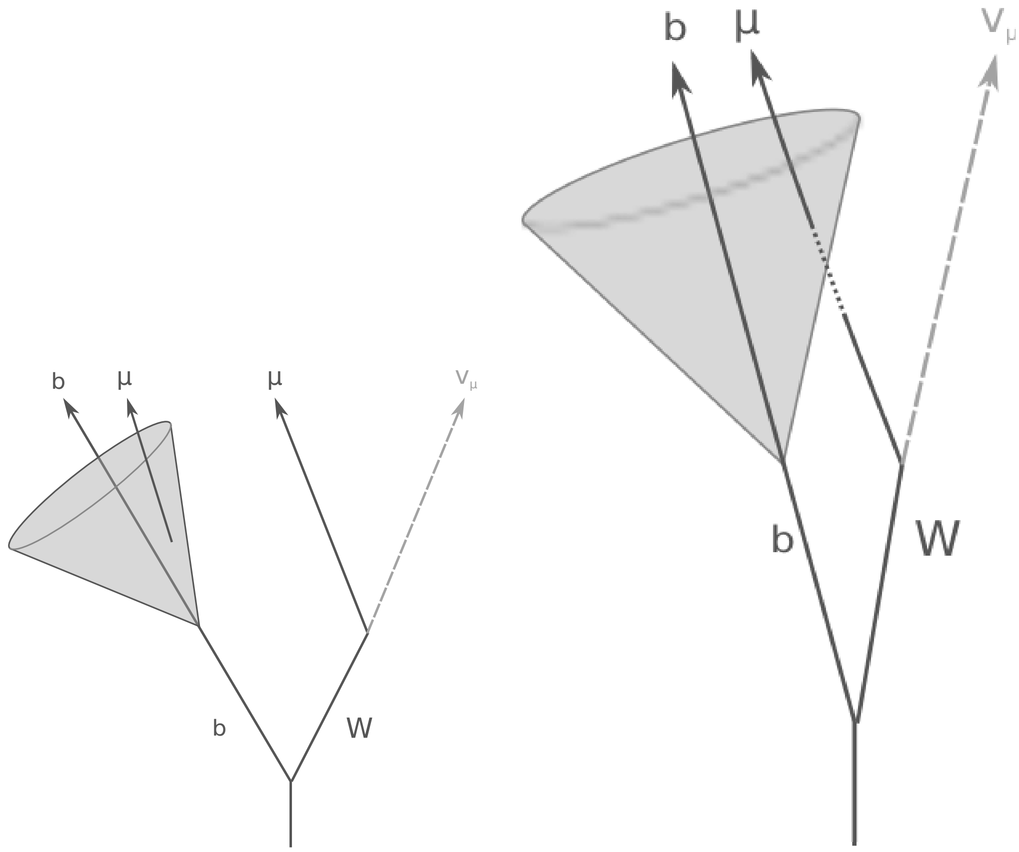

(a) Non-boosted event (b) Boosted event

Figure 8.1: This figure shows a simple diagram for the possible configuration of final-state objects in a (a) boosted and (b) non-boosted events. Note that in both cases a muon is embedded within the b-jet

are collimated.

As can be seen from Fig. 8.2 the increase in boost does result in the W muon and b-quark emerging closer. Note that the fraction of events below the SMT requirement of $\Delta R(\mu, jet) < 0.5$ increases with increased top-quark p_{T}. Additionally Fig. 8.3 shows that the top p_{T} distribution peaks at just below half of the mass of the Z' boson, thus the large portion of the candidate muons in the sample will pass the aforementioned separation requirement. The decay products of the top quark appear to emerge primarily back to back as seen in Fig. 8.4.

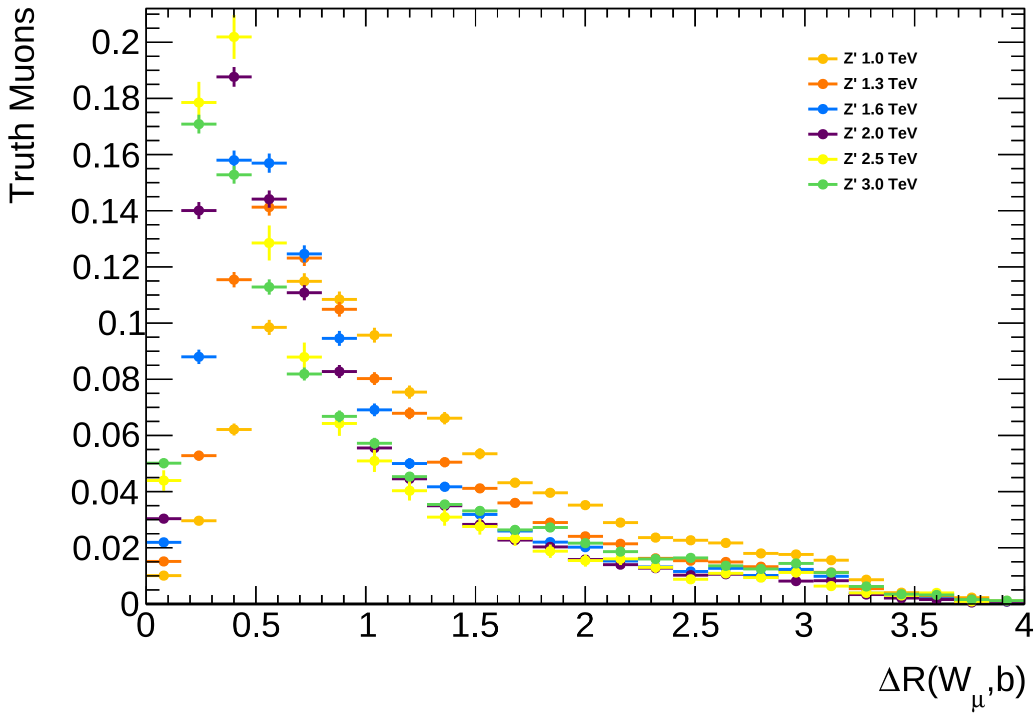

Figure 8.2: The angular separation (ΔR) between the truth W muon and the corresponding b-quark for all examined Z' mass points.

8.2 Samples and muon selection

This measurement is based on simulated data generated for a Z' with a mass of 1.0, 1.3, 1.6, 2.0, 2.5 and 3.0 TeV. All Monte Carlo (MC) samples were generated using PYTHIA with CTEQ6LI PDFs. The width of the generated Z' is 3% of the mass.

8.3 Signal muon selection

8.3.1 Muon selection

The nominal muon object selection includes an isolation requirement, which normally removes events where the signal lepton is found in a region of the calorimeter with large amounts of activity. Cutting on the amount of energy deposited in the calorimeter around the lepton is an example of one such requirement. Such a cut forms part of the object selection used in the top cross-section measurement described in Part 6.

However, as described a priori, boosted top events result in large collimated jets

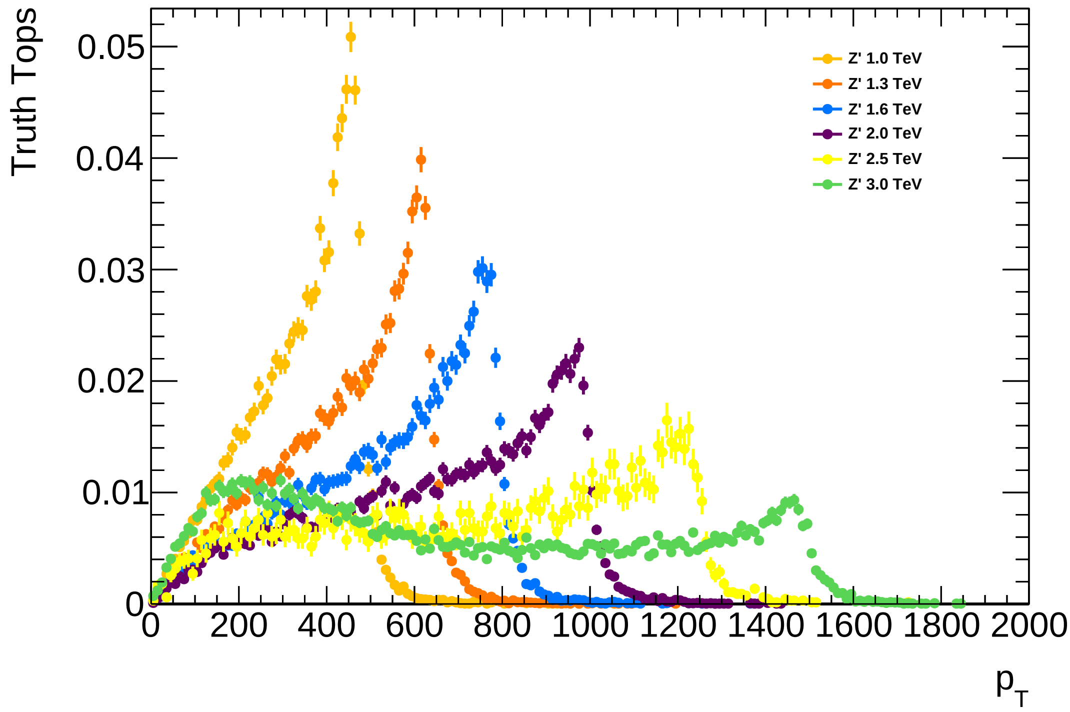

Figure 8.3: The transverse momentum of the top/anti-top quarks in the event for all examined Z' mass points.

which include the products of the two top quarks. Thus the signal lepton can emerge within the cone of the reconstructed jet from the b-quark.

Note that the muon is not required to be isolated, instead the muon is tagged by the χ^2_{match} tagger. Selecting isolated muons would reduce significantly the number of muons available for tagging. Additionally, as explained a priori, events which exhibit stronger collimation are more likely to emerge from particles with higher masses. By requesting the muons be isolated, the ability to probe those higher mass events is diminished.

Another candidate to replace the traditional isolation selection is the so-called mini-isolation. This variable takes into account the strong collimation of the top products with increasing boost. Mini-isolation is defined as the sum of the measured transverse momenta of all tracks in a cone of size of size $\Delta R = k_T/p_T^\ell$ around the lepton, where k_T is an adjustable scale and p_T^ℓ is the momentum of the lepton in question. This is known as the absolute mini-isolation. This study uses the relative mini-isolation where the absolute value is scaled by the momentum of the lepton (MI/p_T^ℓ).

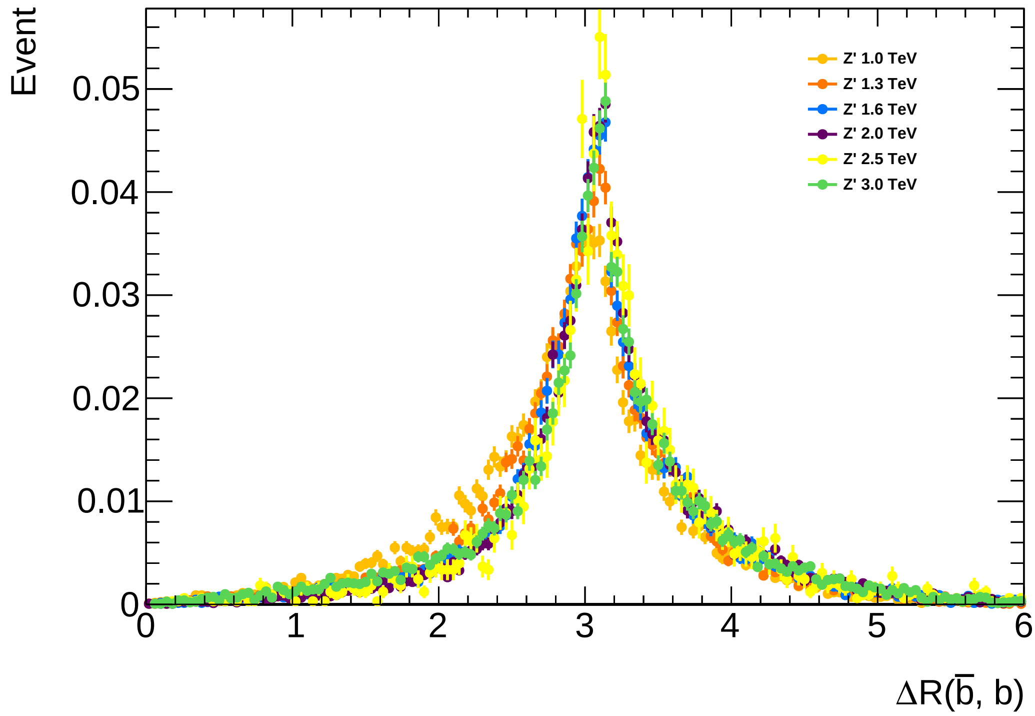

Figure 8.4: The angular separation (ΔR) between the b and $\bar{b}$ in the event for all examined Z' mass points.

In this analysis the performance of the χ^2_{match} tagger is measured against mini-isolation using a $k_T = 10$ and a lepton is deemed isolated if the p_T in the MI cone is less than 5% that of the lepton. The Muon Tagger operates with the same selection as used in Part 6, the cuts are $|z_0| < 3.0$ mm, $|d_0| < 3.0$ mm and finally $\chi^2_{\text{DoF}} < 3.2$.

Thus two separate selections are applied, one for for mini-isolation and one for SMT. Note that both methodologies have different muon reconstruction criteria, these are detailed in Table 8.1.

Table 8.1: Muon reconstruction selection used by Mini-Isolation and by Muon Tagging

Mini-Isolation	Muon-Tagging
MCP Cuts	
$p_{\text{T}} > 20$ GeV	
$\|\eta\| < 2.5$	
MUID	STACO
$z_0 < 3.0$ mm	Is Combined Muon
IsEM Tight	

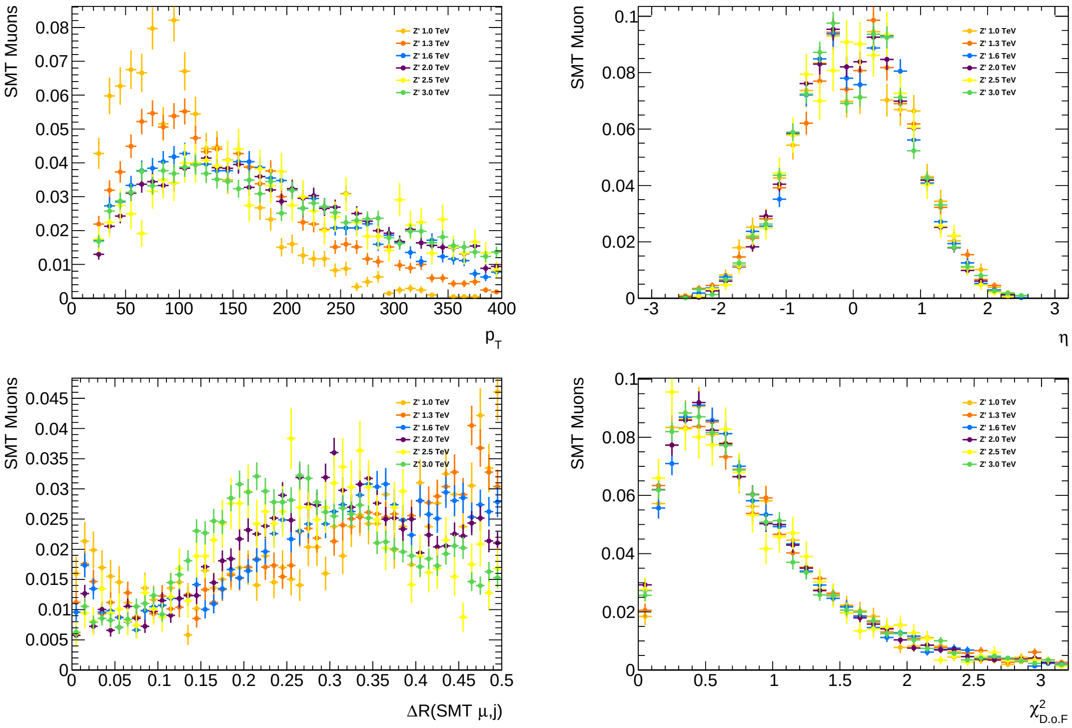

Figure 8.5: This figure shows the distribution of (a) transverse momentum and (b) pseudo-rapidity of muons which pass the SMT selection, the (c) angular separation between those muons and the nearest jet in th event and (d) the χ^2_{match} used in the selection for all tested Z' mass points.

The performance of both methodologies are then compared by measuring their efficiency.

8.4 Efficiency definition

The efficiency measurement was designed to provide an accurate representation of the performance of the soft muon tagger and a valid comparison with mini-isolation. Additional sources of inefficiency such as muon reconstruction are separated out into an additional efficiency which is also quoted. See Fig. 8.7 for a summary of the efficiency measurement.

Firstly, events where a W decays into a muon are selected, this becomes the pool of events from which the efficiency is measured. The selections then diverge and the two sets of reconstruction cuts described in Table 8.1 are applied independently. The

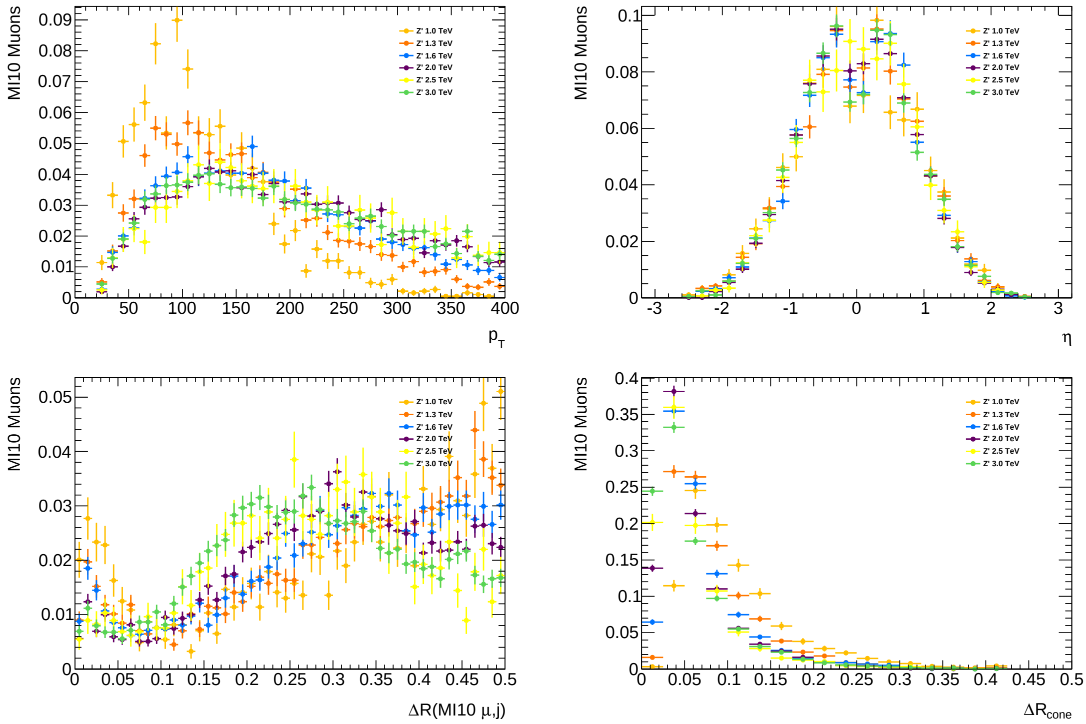

Figure 8.6: This figure shows the (a) transverse momentum and (b) pseudo-rapidity of muons which pass the MI10 selection, the (c) angular separation between those muons and the nearest jet in th event and (d) the cone size used in the selection for all tested Z' mass points.

efficiency of each sets of reconstruction cuts are measured as:

$$\epsilon_{\text{reco}} = \frac{\text{Muons which pass selection}}{\text{All reconstructed muons}}$$

These good reconstructed muons are then truth-matched to the truth μ from the W if the angular separate (ΔR) between them is less than 0.01. This has an efficiency associated with it, defined as:

$$\epsilon_{\text{match}} = \frac{\text{Muons matched to truth } W \text{ muon}}{\text{Muons which pass selection}}$$

Note that at each stage the denominator is the numerator of the previous efficiency. This allows for a combination of all the efficiencies to obtain an inclusive measure which can used to approximate the number of W muons which would be selected from collision data assuming that the simulation describes the data well.

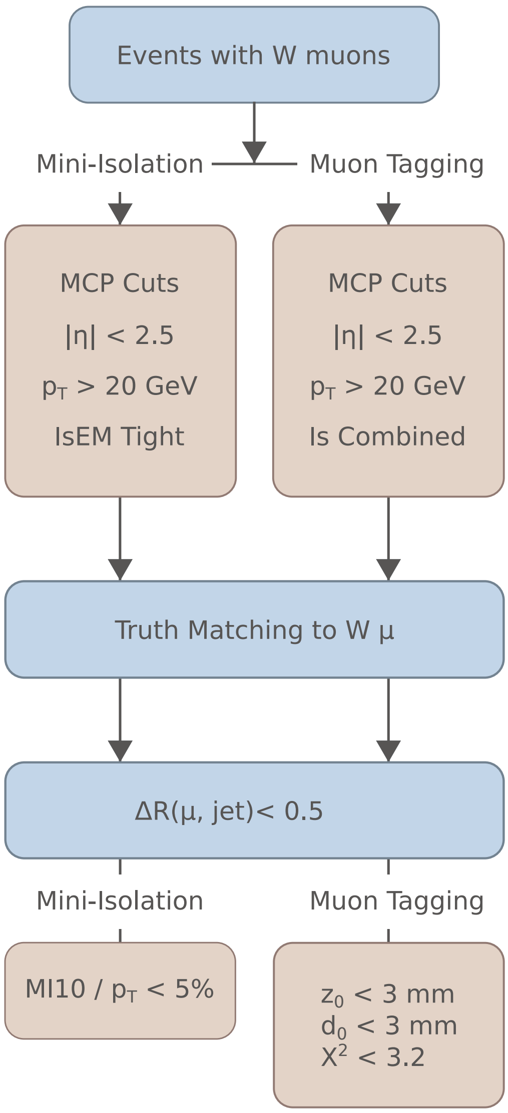

[th!]

Figure 8.7: Structure of the efficiency measurement.

Next the muons are required to be within $\Delta R < 0.5$ from a jet. The Muon Tagger requires that jets be near a jet, in addition the impetus behind the analysis is to probe highly boosted events exploiting the capabilities of χ^2_{match} tagging. This selection ensures that the muons available for χ^2_{match} tagging are indeed close to a jet. This selection also has an efficiency associated with it defined as:

$$\epsilon_{\text{non-iso}} = \frac{\text{Muons with }\Delta\text{R}(\mu,\text{ jet})<0.5}{\text{Muons matched to truth }W\text{ muon}}$$

The final step is the application of both the mini-isolation selection and the muon tagging selection discussed a priori. These selections are associated with the final and most interesting sets of efficiencies, defined as:

$$\epsilon_{\mathrm{MT/MI10}} = \frac{\text{Muons which pass MT/MI10 selection}}{\text{Muons with } \Delta\mathrm{R}(\mu, \text{ jet})<0.5}$$

Please note that the denominator in every efficiency is a subset of the previous denominator. In other words each selection is applied in sequence and the efficiencies are calculated out of the remaining muons which passed the previous selection criteria.

Note that in the nominal analysis described in [3] muons which are within ΔR of 0.1 of the jet would be removed. The impetus behind the analysis is to exploit the χ^2_{match} tagger to accept additional events where the signal muon emerges very close to the jet axis, thus overlap removal is not part of the χ^2_{match} tagging selection. In order to provide an accurate performance comparison between the χ^2_{match} tagger and mini-isolation, the overlap removal is applied only for the mini-isolation selection at the end of the chain. The additional acceptance gained by using χ^2_{match} tagger is compared to the mini-isolation selection with overlap included:

$$\epsilon = \frac{\text{Muons that pass } \chi^2_{\mathrm{match}} \text{ tagger - MI muons } \Delta \text{ R}<0.1}{\text{Total } W \ \mu} \tag{8.1}$$

8.5 Results

Mini-isolation is a very efficient method for selecting muons. Table 8.2 shows the efficiency for the χ^2_{match} tagger, mini-isolation and mini-isolation including overlap removal. Across the used mass range, the efficieny of selection remains above 80% and in fact increases with a increased Z' mass. When the Z' has a mass of 3 TeV the efficiency of selection with mini-isolation is 92.5% with no overlap removal. In contrast the efficiency of the χ^2_{match} tagger is more consistent across the used mass range and higher than mini-isolation for a given mass. For a Z' with a mass of 3 TeV the measured efficiency of the χ^2_{match} tagger is 96.2%. When applying the overlap removal the efficiency of mini-isolation falls to 85.0%. As can be seen from Fig. 8.8 the efficiency of mini-isolation dips for muons which are close to a jet however this occurs below the threshold of the overlap removal. Finally the additional acceptance gained as defined in 8.1 is 4.03%.

Z' Mass [TeV]	χ^2_{match}	MI10	MI10 + Overlap
1.0	94.9%	83.1%	67.0%
1.3	95.8%	89.0%	79.2%
1.6	95.9%	90.4%	81.9%
2.0	96.0%	92.4%	85.7%
2.5	95.8%	92.8%	85.1%
3.0	96.2%	92.5%	85.0%

Table 8.2: Efficiency of selecting a muon by using the χ^2_{match} tagger against mini-isolation. Note that 'MI10 + Overlap' is the efficiency of applying both the mini-isolation cut and overlap removal.

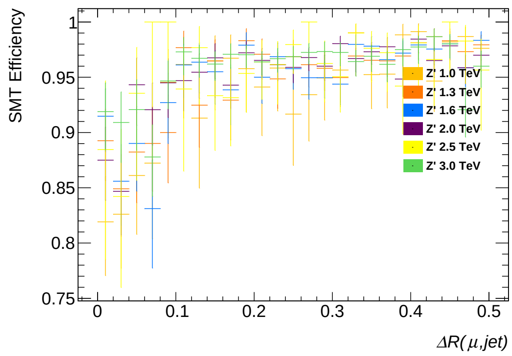

(a) χ^2_{match} muon tagger

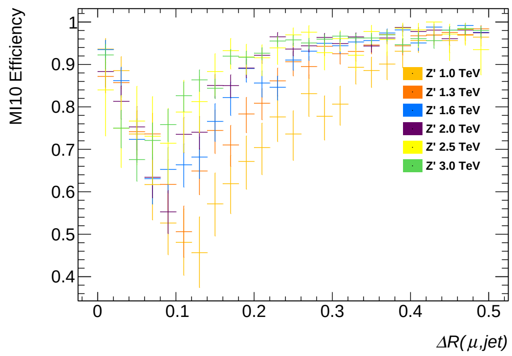

(b) Mini-isolation with $k_T = 10$

Figure 8.8: Efficiency of mini-isolation ($k_T = 10$) and χ^2_{match}muon tagger as a function of the angular separation between the reconstructed muon and the nearest reconstructed jet. Note the dip in the mini-isolation efficiency at low ΔR. In the nominal analysis an overlap removal between the jet and the muon is applied.

The additional acceptance gained in all mass points is also included in Table 8.2.

8.5.1 Background

A preliminary examination of the amount of background was performed. This was done on the same sample of events but instead of selecting semileptonic events, the all-hadronic events are used as background. While these events do not perfectly mimic the true background, namely $b\bar{b}$, the lack of any real signal muons can provide a suitable preliminary substitute.

The lack of an isolation requirement is expected to result in a substantial increase in the amount of background selected. Additionally the semileptonic b-decays in $b\bar{b}$ would result in muons that the χ^2_{match} tagger will select. The analysis chain described

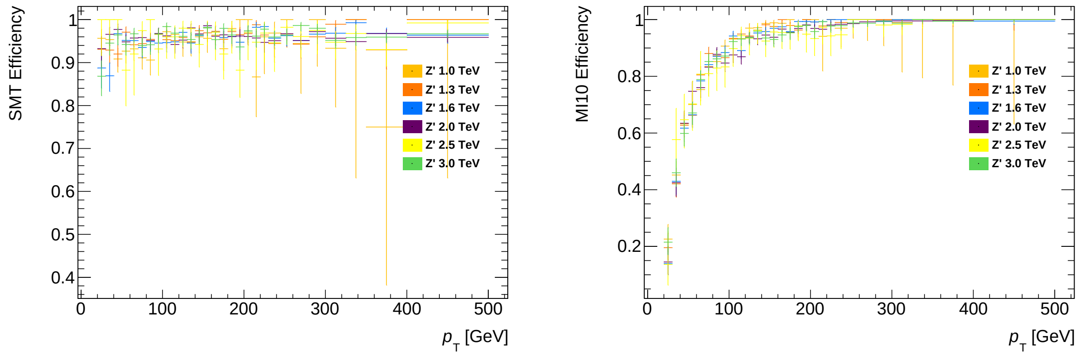

(a) χ^2_{match} muon tagger (b) Mini-isolation with $k_T = 10$

Figure 8.9: Efficiency of mini-isolation ($k_T = 10$) and χ^2_{match}muon tagger as a function of the transverse momentum of the muon.

in Section 8.4 is repeated on the same sample used a priori however the truth level selection of events with a W muon is reversed, thus at truth level both W bosons decay hadronically.

The results of this selection are presented in Table 8.3. As expected mini-isolation removes a substaintial amount of background while maintaining very high signal efficiency. In comparison, removing the isolation requirement greatly increases the background acceptance when using the χ^2_{match} tagger. A full treatment of the background would be required to account for the background present.

The increase in signal acceptance does not make this methodology sufficiently advantageous particularly when considering the increase in fake rate. An examination of the b-tagging potential of the χ^2_{match} tagger is presented in the next section.

Table 8.3: Fake rate of χ^2_{match} tagger, mini-isolation and mini-isolation including overlap removal as measured using all Z' mass points.

Z' Mass [TeV]	χ^2_{match}	MI10	MI10 + Overlap
1.0	92.8%	4.10%	2.39%
1.3	92.4%	4.77%	3.66%
1.6	91.8%	5.46%	4.55%
2.0	91.1%	7.07%	6.09%
2.5	90.0%	6.40%	5.57%
3.0	90.1%	6.59%	5.68%

Table 8.4: caption

Z' Mass [TeV]	Good Muons	Matched Muons	$\Delta R(\mu, jet) < 0.5$	χ^2_{match}-tagged
1.0	16382	9807 (59.8%)	8722 (88.9%)	8237 (94.4%)
1.3	21099	13344 (63.2%)	12083 (90.6%)	11402 (94.4%)
1.6	19947	13012 (65.2%)	11929 (91.7%)	11240 (94.2%)
2.0	23391	15235 (65.1%)	14177 (93.1%)	13276 (93.6%)
2.5	5152	3347 (64.9%)	3137 (93.7%)	2922 (93.1%)
3.0	21766	13835 (63.5%)	13032 (94.2%)	12145 (93.2%)

8.6 B-tagging potential in boosted events

Chapter 9

Conclusions

Appendices

Appendix A

List of triggers used in calibration

The calibration analysis makes use of an OR of the triggers listed below. The triggers fire based on a set of criteria summarized in the trigger name following the ATLAS trigger naming convention. The list includes generic single low-p_T muon triggers such as `EF_mu6` and `EF_mu15`, single high-p_T muons & jets triggers such as `EF_mu24_j65_a4tchad` and the specialized J/ψ trigger `EF_mu6_Trk_Jpsi_loose`.

- `EF_mu24_j65_a4tchad_EFxe40_tclcw`
- `EF_mu4T_j65_a4tchad_xe60_tclcw_loose`
- `EF_mu24_j65_a4tchad`
- `EF_mu18_tight_e7_medium1`
- `EF_mu4T_j65_a4tchad_xe70_tclcw_veryloose`
- `EF_mu24_j65_a4tchad_EFxe60_tclcw`
- `EF_mu24_tight_b35_mediumEF_j35_a4tchad`
- `EF_mu20i_tight_g5_loose_TauMass`
- `EF_mu6_Trk_Jpsi_loose`
- `EF_mu24i_tight`
- `EF_mu24i_tight_MuonEF`

- EF_mu24i_tight_MG
- EF_mu24i_tight_l2muonSA
- EF_mu24_tight_3j35_a4tchad
- EF_mu24_g20vh_loose
- EF_mu40_MSonly_barrel_tight
- EF_mu50_MSonly_barrel_tight
- EF_mu24_tight_EFxe40
- EF_mu24_tight_L2StarB
- EF_mu18_medium
- EF_mu24_medium
- EF_mu24_tight
- EF_mu24_tight_MuonEF
- EF_mu24_tight_MG
- EF_mu24_tight_L2StarC
- EF_mu36_tight
- EF_mu40_tight
- EF_mu20it_tight
- EF_mu24_g20vh_medium
- EF_mu18_2g10_medium
- EF_mu24_muCombTag_NoEF_tight
- EF_mu10i_loose_g12Tvh_medium
- EF_mu10i_loose_g12Tvh_medium_TauMass

- EF_mu18_2g10_loose
- EF_mu10i_g10_medium_TauMass
- EF_mu20i_tight_g5_medium_TauMass
- EF_mu24_tight_3j45_a4tchad
- EF_mu24_tight_4j45_a4tchad
- EF_mu24_tight_4j35_a4tchad
- EF_mu4T
- EF_mu6
- EF_mu15
- EF_mu40_slow_tight
- EF_mu60_slow_tight1
- EF_mu22_IDTrkNoCut_tight
- EF_mu8_4j45_a4tchad_L2FS
- EF_mu6_Trk_Jpsi_loose_L2StarB
- EF_mu6_Trk_Jpsi_loose_L2StarA
- EF_mu24_j65_a4tchad_EFxe40wMu_tclcw
- EF_mu24_j65_a4tchad_EFxe60wMu_tclcw
- EF_mu6T_2b55_medium_2j55_a4tchad_L1J20_matched
- EF_mu24i_tight_muFast
- EF_mu4T_L2StarB
- EF_mu6_L2StarB
- EF_mu15_vbf_L1TAU8_MU10

Appendix B

List of combined muon performance (MCP) cuts

Bibliography

[1] A search for $t\bar{t}$ resonances in the lepton plus jets final state with ATLAS using 14 fb^1 of pp collisions at $\sqrt{s} = 8$ TeV. Technical Report ATLAS-CONF-2013-052, CERN, Geneva, May 2013. Not published in the proceedings.

[2] Search for $t\bar{t}$ resonances in semileptonic final state. Technical Report CMS-PAS-B2G-12-006, CERN, Geneva, 2013.

[3] Georges Aad et al. Search for $t\bar{t}$ resonances in the lepton plus jets final state with ATLAS using 4.7 fb^{-1} of pp collisions at $\sqrt{s} = 7$ TeV. *Phys.Rev.*, D88(1):012004, 2013.

[4] Serguei Chatrchyan et al. Search for anomalous $t\bar{t}$ production in the highly-boosted all-hadronic final state. *JHEP*, 1209:029, 2012.

[5] Serguei Chatrchyan et al. Search for Z' resonances decaying to $t\bar{t}$ in dilepton+jets final states in pp collisions at $\sqrt{s} = 7$ TeV. *Phys.Rev.*, D87:072002, 2013.